Magnetic penetration depth in Nb/Al and Nb/Cu superconducting proximity bilayers

R. F. Wang, S. P. Zhao, G. H. Chen, and Q. S. Yang
Institute of Physics and Center for Condensed Matter Physics, Chinese Academy of Sciences, Beijing 100080, People's Republic of China
(Received 14 June 2000)

Magnetic penetration depth λ in Nb/Al and Nb/Cu superconducting bilayers, its absolute values and temperature dependencies under the variations of material and sample parameters are systematically investigated. Measurements of λ are performed by using the two-coil mutual inductance technique and the results are compared with a recent microscopic theory [Phys. Rev. B **59**, 14 630 (1999)] based upon Eilenberger-Usadel's quasiclassical equations of superconductivity. Our results show that the $\lambda(T)$ characteristics at low temperatures usually follow a power law, or a linear temperature dependence, if the sublayer thicknesses are less than several times of their coherence length and the interface resistance is small. A two-gap, steplike feature in the $\lambda(T)$ curve of the Nb/Al bilayer system will develop around the sublayer transition temperature of Al when the interface resistance increases or when the Al layer thickness becomes much larger than its coherence length. These results can be well described within the framework of the microscopic theory.

I. INTRODUCTION

Recently there have been several experimental[1–5] and theoretical[6,7] studies of magnetic penetration depth λ in conventional layered superconductors (bilayers or multilayers). Experimental results from the microwave surface impedance measurements,[1–3] the two-coil mutual inductance measurements,[4] and the ac susceptibility measurements[5] indicated that the $\lambda(T)$ curve can have a linear or sublinear temperature dependence or obey a power law, which are different from the behavior of the bulk homogeneous superconductors.

Proximity-induced alternation of the superconducting properties along the direction z perpendicular to the layer planes is believed to be the cause for these results.[4,6,7] In a phenomenological treatment, Pambianchi *et al.*[7] proposed to evaluate λ in SS' bilayers utilizing a space- and temperature-dependent order parameter $\Delta(z,T)$ (S and S' are usually different superconductors and in this work we shall assume that $T_{c,S} > T_{c,S'} \geqslant 0$). In one of their models, they assumed that in the S' layer, the superconducting order parameter can be described by $\Delta_{S'}(z,T) \propto \Delta_S(T)\exp(-K_{S'}z)$ where $\Delta_S(T)$ is the BCS potential and is considered to be space-independent. The decay length $K_{S'}^{-1}$ increases with the decrease of temperature[8] and diverges near $T_{c,S'}$, the transition temperature of the S' layer. λ can be related to Δ by $\lambda \sim 1/\Delta$ in the simple cases. Good agreement has been reached between their experiments and model calculations.[1–3]

An alternative treatment, applicable to the λ evaluation for the SS' bilayers and multilayers at the microscopic level, has been developed[6] based on Eilenberger-Usadel's quasiclassical equations.[9,10] In contrast to the approach of Pambianchi *et al.*,[7] which is strictly applicable near the transition temperature T_c of the bilayer system, the microscopic theory provides a description over the entire temperature range below T_c. Most of the parameters required for the λ evaluation in the theory, like the layer thicknesses $d_{S,S'}$, resistivities $\rho_{S,S'}$, and transition temperatures $T_{c,S,S'}$, can be known directly from experiments. Numerical results from the model calculation have revealed many of the experimentally observed $\lambda(T)$ features.

We have recently demonstrated that the two-coil mutual inductance technique, first developed by Fiory *et al.*,[11] can be used to measure the absolute value of λ directly for the superconducting thin films.[12] It will therefore be interesting to test the microscopic theory using the experimental λ data, especially the low temperature data around and below $T_{c,S'}$, which are previously not studied experimentally.

In this paper, we present our experimental results on a series of Nb/Al and Nb/Cu bilayers. We will focus on the low temperature data and their comparison with the theoretical prediction under the variations of the sample and material parameters including $d_{S,S'}$, $\rho_{S,S'}$, $T_{c,S,S'}$, as well as the interface resistance R_B of the bilayers. Since the two-coil technique requires a partial penetration of the magnetic field through the sample film, the film thickness should be limited in order to have a high accuracy in the measurements.[12] A second limitation for the samples comes from the theoretical side. Namely, one of the layers in an SS' sandwich should be thin compared to its coherence length ξ so that the superconducting properties can be considered to be constant across the layer. We shall present our experimental details and the theoretical background in Sec. II and Sec. III, respectively. Experimental results and discussion will be given in Sec. IV. Section V is a summary.

II. EXPERIMENTAL DETAILS

Our Nb/Cu and Nb/Al bilayer samples were prepared in an ultrahigh vacuum system equipped with three dc magnetron sputter targets.[13] The background pressure was 1×10^{-6} Pa. Relatively large single crystal silicon substrates, $16 \times 15 \times 0.5$ mm^3 in sizes and suitable for the penetration depth measurements,[12] were used and carefully cleaned be-

TABLE I. Parameters for the Nb/Cu and Nb/Al bilayers ($S \rightarrow$Nb, $S' \rightarrow$Al or Cu).

S/S'	d_S (nm)	ρ_S ($\mu\Omega$ cm)	$d_{S'}$ (nm)	$\rho_{S'}$ ($\mu\Omega$ cm)	T_c^{expt} (K)	T_c^{calc} (K)	ξ_S (nm)	$\xi_{S'}$ (nm)	γ_M	λ_e (nm,	λ_t 1.6 K)
Nb/Al	20	21.8	10	7.01	7.43	7.36	5.06	20.7	0.369	121	149
(Group A)			20	4.95	7.14	7.04	5.17	25.1	0.721	103	130
			30	2.21	6.84	6.79	5.26	38.3	1.06	83.9	92.2
			40	2.10	6.79	6.63	5.33	39.8	1.40	77.8	91.0
Nb/Cu	20	21.8	10	5.21	7.20	7.28	5.08	28.5	0.261	132	139
(Group B)			20	3.82	6.74	6.91	5.22	34.2	0.509	118	122
			30	2.54	6.71	6.67	5.31	42.7	0.751	110	104
			40	1.94	6.38	6.49	5.38	49.5	0.987	105	94.8

fore sputter deposition. Nb films were usually deposited first with a deposition rate of 2 nm/s. Then the substrates were transferred to the Al or Cu target, and the Al or Cu films were sputtered onto the Nb films with the rates of 0.4 or 2 nm/s, respectively.

We have prepared five groups of samples (Groups A to E), the sample parameters of which are summarized in Table I and Table II. Groups A (Nb/Al) and B (Nb/Cu) were prepared under a sputter pressure of 1.5 Pa in pure Ar (99.999%), while in the preparation of the Nb/Al samples of Groups C to E, a small amount of O_2 gas ($\sim$0.068–0.073 Pa) was introduced into the chamber right after the deposition of the Nb films. In the latter case, the Nb film surface was allowed for oxidation in the Ar+O_2 mixture for a given time period of t_o. Then the Al film was sputtered onto the Nb film in the mixture gas. There were two purposes for adding the O_2 gas in this work. One was to oxidize the Nb film surface and increase the interface resistance between the two layers. The other was to increase the resistivity as well as the transition temperature of the Al film. The lowest temperature we could reach in our experiments was about 1.6 K, which is above $T_{c,\text{Al}}$ of pure Al of 1.2 K. If we want to observe the feature of λ in Nb/Al bilayers around $T_{c,\text{Al}}$, $T_{c,\text{Al}}$ must be higher than 1.6 K. Our measurements showed that $T_{c,\text{Al}}$ could reach 2.0 K if it was prepared in the gas mixture mentioned above.

The film thicknesses were measured from a DEKTAK Scan Profiler. The resistivity ρ and transition temperature T_c for the Nb films and Nb/Al and Nb/Cu bilayers were measured independently using the standard four-point technique (T_c was also determined from the mutual inductance data, see Fig. 1). The resistivity for the Al or Cu film in a bilayer was evaluated considering the bilayer as two parallelly connected thin-film resistors. Since the thicknesses of the Nb films used in our experiment were thin (10 or 20 nm), their transition temperatures, sensitive to the film thickness and surface condition, could vary by 0.1–0.3 K for the samples of different groups. These data are not listed in Table I and Table II but will be discussed in Sec. IV A.

The penetration depth λ was measured by the two-coil inductance technique which has been described earlier.[12] Using this technique, we were able to determine the absolute value of λ with high accuracy by converting the mutual inductance data M according to

$$\frac{M}{M_e} = \frac{\alpha}{M_e}\frac{\lambda^2}{d} + \frac{\beta}{M_e},$$

where M_e is the mutual inductance without the film, α is a geometric factor, and β is the baseline. Due to the relatively thin Nb thickness in the bilayer samples, special care has been taken in this work to take the data below a temperature T_0 above which significant dissipation process occurs. In Fig. 1, typical mutual inductance data (both in-plane and quadrature components), obtained in a Nb/Al sandwich, are shown.

III. THEORETICAL BACKGROUND

For a superconducting bilayer SS' with S and S' both in the dirty limit, its properties can be described within the

TABLE II. Parameters for the Nb/Al bilayers with nonzero interface resistance.

d_{Nb} (nm)	ρ_{Nb} ($\mu\Omega$ cm)	d_{Al} (nm)	ρ_{Al} ($\mu\Omega$ cm)	t_o (sec)	T_c^{expt} (K)	R_B ($\mu\Omega\text{cm}^2$)	T_c^{calc} (K)	ξ_{Nb} (nm)	ξ_{Al} (nm)	γ_M	γ_B	λ_e (nm,	λ_t 2.1 K)
10	30.0	60	50.0[a]	5	6.20	1×10^{-4}	6.41	4.61	8.27	6.49	15.7	511	455
(Group C)				20	6.65	1.5×10^{-3}	6.89	4.44	7.98	6.73	253	575	547
				35	6.79	4×10^{-3}	6.93	4.43	7.96	6.75	679	578	571
				300	6.71	2.5×10^{-1}	6.95	4.43	7.94	6.76	4.26×10^{4}	576	586
10	30.0	60	25.0[a]	10	6.64	1×10^{-4}	6.48	4.59	11.7	4.61	15.8	297	367
(Group D)				15	6.74	5×10^{-4}	6.93	4.44	11.3	4.76	84.5	415	444
				20	6.85	2×10^{-3}	7.05	4.40	11.2	4.80	344	505	520
10	30.0	30	45.6	5	7.00	3×10^{-4}	6.99	4.42	8.31	6.46	51.1	289	370
(Group E)		120			6.89	3×10^{-4}	6.99	4.42	8.31	6.46	51.1	590	634

[a]The exact resistivity data ρ_{Al} in groups C and D were obtained from fitting to the experimental data. See Ref. 14.

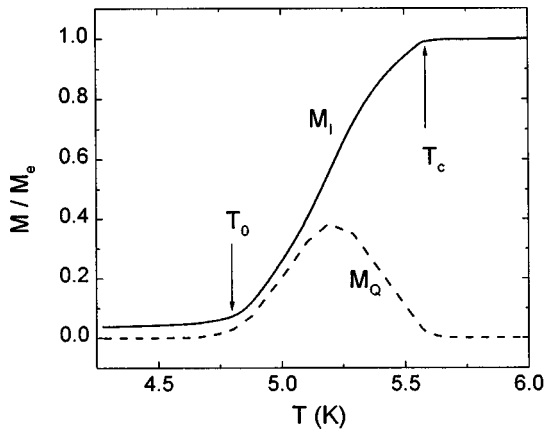

FIG. 1. Normalized mutual inductance data for a Nb/Al bilayer with parameters similar to the first sample of group D in Table II but with a smaller Nb thickness (8–9 nm) showing a wider dissipation region $\Delta T = T_c - T_0$. M_I and M_Q correspond to the in-plane and quadrature components, respectively. T_c indicated here corresponds to the zero resistance temperature in the four-point resistivity measurements.

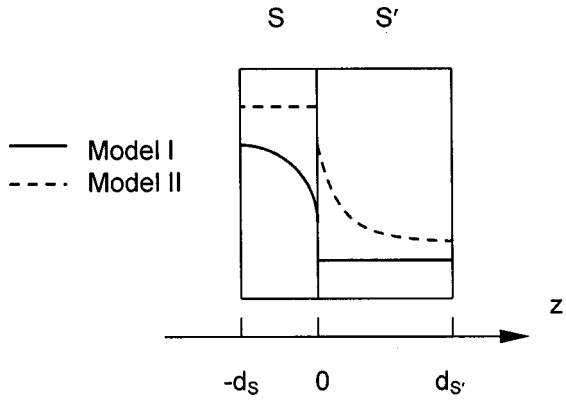

FIG. 2. Spatial variations of the superconducting order parameter in SS' sandwiches ($T_{c,S} > T_{c,S'} \geq 0$). Model I (II) corresponds to the case in which the S' (S) layer thickness is less than its coherence length.

framework of Usadel's equations,[10] which are the dirty-limit version of Eilenberger's theory.[9] In particular, it is shown that, by employing the boundary conditions first developed by Kuprianov and Lukichev,[15] the transition temperature T_c of the bilayer is determined by the following transcendental equation:[6]

$$\rho_S q_{S'} \tanh(q_{S'} d_{S'}) - \rho_{S'} q_S \tan(q_S d_S) = R_B q_S q_{S'} \tanh(q_{S'} d_{S'}) \tan(q_S d_S), \quad (1)$$

where R_B is measured in resistance times area at the interface, and $q_{S,S'}$ are defined by

$$q_{S,S'}^2 = \pm \left(\frac{2\pi k_B T \delta_{S,S'}}{\hbar D_{S,S'}} \right), \quad (2)$$

where $D_{S,S'}$ are the diffusion coefficients, and $\delta_{S,S'}$ are determined by

$$\ln\left(\frac{T}{T_{c,S,S'}} \right) = -2 \sum_{n \geq 0} \left(\frac{1}{2n+1} - \frac{1}{2n+1+\delta_{S,S'}} \right), \quad (3)$$

in which $T_{c,S,S'}$ are the transition temperatures of single S and S' films. If we set $T_{c,S} > T_{c,S'} \geq 0$, then the upper and lower signs in Eq. (2) correspond to the S and S' films, respectively. We note that Eq. (1) returns to the well-known results of de Gennes[16] and Werthamer[17] if $R_B = 0$.

Golubov *et al.*[18] have demonstrated that the superconducting properties in the whole temperature range below T_c can be found within the Eilenberger-Usadel formalism if one of the layers in the SS' sandwich is thin compared to its coherence length so that the superconducting properties are uniform across this layer. In Fig. 2, two soluble situations for the SS' bilayers are shown, which will be referred to as model I and model II in our numerical simulations. In the original treatment of Golubov *et al.*,[18] an infinitely thick S layer is considered so the superconducting order parameter equals the bulk value at the S layer surface. This serves as a boundary condition. Since in our work, both S and S' layers have finite thickness, an alternative boundary condition[19,6] should be used. Let us take model II (see Fig. 2) as an example. If we define

$$G_{S'} = \cos\theta_{S'}, \quad F_{S'} = \sin\theta_{S'}, \quad (4)$$

where $G_{S'}$ and $F_{S'}$ are Gorkov's Green functions integrated over energy and averaged over the Fermi surface, the Usadel's equations reduce to the following equation:[6]

$$\theta''_{S'}(\omega_n, z) + \Delta_{S'}(z) \cos\theta_{S'}(\omega_n, z) - \omega_n \sin\theta_{S'}(\omega_n, z) = 0, \quad 0 \leq z \leq d_{S'}/\xi_{S'}, \quad (5)$$

where a prime denotes a derivative with respect to z and $\omega_n = (2n+1)(T/T_c)$ is Matsubara frequency normalized to $\pi k_B T_c$. z is normalized to $\xi_{S'}$:

$$\xi_{S,S'} = \sqrt{\frac{\hbar D_{S,S'}}{2\pi k_B T_c}} = \sqrt{\frac{\pi \hbar k_B}{6e^2 \rho_{S,S'} \gamma_{S,S'} T_c}}. \quad (6)$$

Here γ is the coefficient of the electronic specific heat. In Eq. (6), we have used

$$D = v_F l/3 = (\pi k_B)^2/(3e^2 \rho \gamma), \quad (7)$$

in which l and v_F are the mean free path and Fermi velocity. The boundary conditions read

$$\theta'_{S'}(\omega_n, d_{S'}) = 0, \quad (8)$$

$$\theta'_{S'}(\omega_n, 0) = \frac{\gamma_M [\omega_n \sin\theta_{S'}(\omega_n, 0) - \Delta_S \cos\theta_{S'}(\omega_n, 0)]}{\{1 + \gamma_B^2(\omega_n^2 + \Delta_S^2) + 2\gamma_B [\omega_n \cos\theta_{S'}(\omega_n, 0) + \Delta_S \sin\theta_{S'}(\omega_n, 0)]\}^{1/2}}, \quad (9)$$

in which γ_B describes the coupling strength, while γ_M is a measure of the strength of the proximity effect, between S and S' layers:

$$\gamma_B=\frac{R_B}{\rho_S\xi_S}\frac{d_S}{\xi_S},\quad \gamma_M=\frac{\rho_{S'}\xi_{S'}}{\rho_S\xi_S}\frac{d_S}{\xi_S}. \tag{10}$$

The order parameters $\Delta_{S,S'}$ are given by the recurrency expressions:

$$\Delta_{S'}^{m+1}(z)=V_{S'}N_{S'}(0)\frac{2T}{T_c}\sum_{\omega_n>0}^{\omega_{D,S'}}F_{S'}^m(\omega_n,z), \tag{11a}$$

$$F_{S'}^m(\omega_n,z)=\sin\theta_{S'}^m(\omega_n,z), \tag{11b}$$

$$\Delta_S^{m+1}=V_SN_S(0)\frac{2T}{T_c}\sum_{\omega_n>0}^{\omega_{D,S}}F_S^m(\omega_n), \tag{12a}$$

$$F_S^m(\omega_n)=\left[1+\left(\frac{\cos\theta_{S'}^m(\omega_n,0)+\gamma_B\omega_n}{\sin\theta_{S'}^m(\omega_n,0)+\gamma_B\Delta_S^m}\right)^2\right]^{-1/2}, \tag{12b}$$

in which $\omega_{D,S,S'}$ are Debye frequencies of the individual layers, and $[VN(0)]_{S,S'}$ are the BCS coupling constants.

We see that for given $d_{S,S'}$, $\rho_{S,S'}$, $T_{c,S,S'}$ and R_B, T_c can be computed from Eqs. (1)–(3). $\xi_{S,S'}$, and therefore γ_B and γ_M can be obtained from Eqs. (6) and (10). With these parameters, Eq. (5) can be solved using the boundary conditions and the expressions for $\Delta_{S,S'}$ which are given by Eqs. (8) and (9) and Eqs. (11) and (12), respectively. For model I shown in Fig. 2, the procedure is exactly the same if we set z axis in the opposite direction and interchange the subscripts S and S' in the above formalism. As is shown in Ref. 6, the penetration depth is given by the following expression:[20]

$$\frac{1}{\lambda_{S,S'}^2}=\frac{4\pi\mu_0k_BT}{\hbar\rho_{S,S'}}\sum_{\omega_n>0}^{\omega_{D,S,S'}}|F_{S,S'}|^2 \tag{13}$$

where $F_{S,S'}=\sin\theta_{S,S'}$ represent the final results of Eqs. (11b) and (12b) (removing all superscripts). Equation (13) defines the local $\lambda_{S,S'}$ that vary along the z axis. Finally, the (in-plane) penetration depth $\lambda(T)$ for a bilayer is given by

$$\lambda^2(T)=\frac{d_S+d_{S'}}{\int_{-d_S}^{d_{S'}}\lambda_{S,S'}^{-2}(T,z)dz}, \tag{14}$$

which will be used to compare with our experimental results.

IV. RESULTS AND DISCUSSION

Before presenting our experimental data and comparing them with the model calculations, we intend to discuss some of the bilayer parameters and the applicability of the theory outlined in the preceding section. We first consider the electronic mean free path l which can be found from Eq. (7). Using the handbook data of $\gamma=7.3$, 1.36, and 0.97×10^{-4} J/cm^3 K^2 for Nb, Al, and Cu respectively, and $v_F=0.273$, 2.02, and 1.57×10^8 cm/sec for the materials, l for the Nb films in Table I is found to be about 1.7 nm while the values for Al and Cu range from 3.8 to 12.7 nm and from 9.3 to 25 nm, respectively. The coherence length ξ defined by Eq. (6) for the sample films is listed in the table. We see that l/ξ is about 0.32 in the case of Nb, and it ranges from 0.18 to 0.32 for Al and from 0.32 to 0.5 for Cu. Similar considerations can be taken for the samples in Table II from which we find l is 1.2 nm for Nb and is about 0.5 or 1.1 nm for the Al films. These lead to $l/\xi\sim0.27$ in the case of Nb and $l\ll\xi$ in the case of the Al films. Summarizing these results, together with the film thicknesses in the tables, we find that the requirements for the theory to be applicable (see Fig. 2):

$$l_S\ll\xi_S<d_S,\quad l_{S'}<d_{S'}\ll\xi_{S'},\quad \text{for model I}$$

and

$$l_S<d_S\ll\xi_S,\quad l_{S'}\ll\xi_{S'}<d_{S'},\quad \text{for model II}$$

are fairly satisfied for the samples in Table I and Table II, respectively, with an exception of $d_{\mathrm{Nb}}\sim2\xi_{Nb}$ (instead of $d_{Nb}\ll\xi_{\mathrm{Nb}}$) in Table II. However, in the above requirements, $d_{S'}\ll\xi_{S'}$ for model I or $d_S\ll\xi_S$ for model II is to ensure a constant superconducting properties across the S' or S layer, and practically, the conditions $d_{S'}\leqslant\xi_{S'}$ or $d_S\leqslant\xi_S$ could be sufficient.[6] We therefore still use the samples in Table II to test the predictions of model II because the Nb film properties will severely deteriorate by further reducing its thickness below 10 nm.

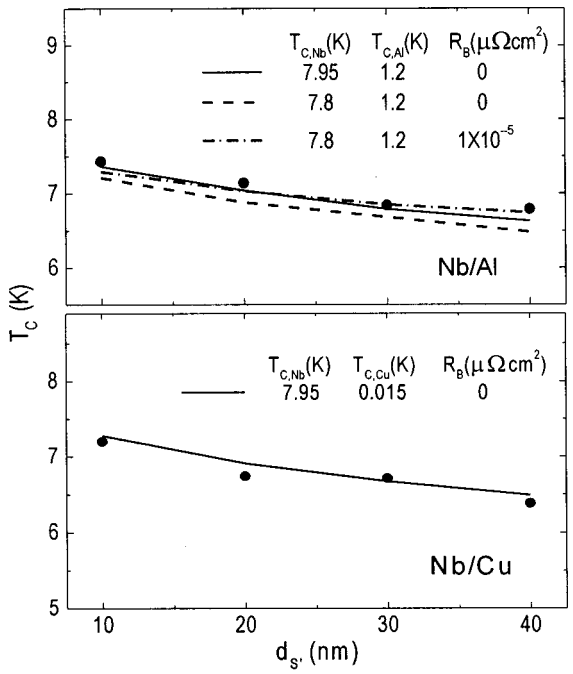

FIG. 3. Transition temperature T_c vs Al (upper) and Cu (bottom) layer thicknesses for the Nb/Al (group A) and Nb/Cu (group B) bilayers. Solid circles are experimental data and the lines are the theoretical results.

A. Transition temperature

In Fig. 3, we show the transition temperature versus Al and Cu layer thicknesses for the Nb/Al and Nb/Cu samples

in Table I (solid circles). The Nb layers have a fixed thickness of 20 nm. The lines in the figure are the theoretical results computed from Eqs. (1)–(3), using the parameters determined from experiments.

In the calculations, the diffusion coefficient D was evaluated from Eq. (7), and the bulk values of $T_{c,\mathrm{Al}}=1.2$ K and $T_{c,\mathrm{Cu}}=0.015$ K were used.[21] For a Nb film with thickness of 20 nm, $T_{c,\mathrm{Nb}}$ can vary noticeably with its thickness as well as its surface condition.[22,12] In order to estimate the effect, we sputtered a single Nb film with a nominal thickness of 22 nm, in expectation of a thin Nb-oxide layer [~ 2 nm (Ref. 23] formed in the air. $T_{c,\mathrm{Nb}}$ for this film was measured to be 7.8 K. The dashed line in Fig. 3 is obtained with $T_{c,\mathrm{Nb}}=7.8$ K and a zero interface resistance $R_B=0$. We find that the calculation results are about 0.2 K below the experimental data. This can be caused by the following two factors. One is that we have neglected the interface resistance R_B. Though R_B should be small, it can still be a nonzero parameter due to the lattice mismatch between the two sublayer films. The other reason is that $T_{c,\mathrm{Nb}}$ has been underestimated due to the uncertainty of the Nb-oxide layer thickness or the further reduction of $T_{c,\mathrm{Nb}}$ through proximity effect in its presence.[22] The dash-dot line is the results with $T_{c,\mathrm{Nb}}=7.8$ K and $R_B=1\times10^{-5}\ \mu\Omega\ \mathrm{cm}^2$, while the solid line is the results with $T_{c,\mathrm{Nb}}=7.95$ K and $R_B=0$. We can see that both lines are closer to the experimental data. In the following, we shall use, for simplicity, $T_{c,\mathrm{Nb}}=7.95$ K and $R_B=0$ for the samples in Table I. The results computed with these parameters for the Nb/Cu bilayers are also shown as a solid line in Fig. 3.

The agreement between theory and experiment seems to be good for the samples in Table I with discrepancies around or below 0.1 K, corresponding to our maximum experimental uncertainty. For the samples in Table II, of which the Nb films with smaller thickness of 10 nm were all subjected to oxidation to have a nonzero R_B, the agreement is less satisfactory with discrepancies reaching 0.24 K in the worst cases, as can be seen in the table. The main reason for this is that we had a less controllable $T_{c,\mathrm{Nb}}$ in the case of the 10-nm thick Nb films, especially with the oxidation process (our experiments lasted for about four months during which the temperatures of the cooling water and working gases changed so that the sputter and oxidation conditions could vary slightly). Previous studies indicate that for the 10-nm thick Nb films, the change in $T_{c,\mathrm{Nb}}$ can be as large as 0.3 K with a thickness change of 1 nm.[23,22] In our case, $T_{c,\mathrm{Nb}}$ for a single, nominally 12-nm thick Nb film was 6.95 K. $T_{c,\mathrm{Nb}}$ for the samples of Groups C, D, and E in Table II was chosen to be 6.95, 7.10, and 7.25 K, respectively, which led to the reasonable fits of both T_c and λ data. $T_{c,\mathrm{Al}}$ in these groups was 2.0 K, as determined from the downturn point in the $\lambda(T)$ curves with largest R_B.

B. Penetration depths in the case of $R_B=0$

In Fig. 4, we show the experimental $\lambda(T)$ data (solid dots), normalized to $\lambda(1.6\ \mathrm{K})$, of the samples in Groups A and B. The absolute values of $\lambda(1.6\ \mathrm{K})$ are listed in Table I. The $\lambda(T)$ curves at low temperatures appear relatively flat for thinnest Al- or Cu-layer samples in the groups, but they already deviate clearly from the bulk exponential behavior due to the proximity effect. For larger Al or Cu layer thickness, λ increases faster with the increase of temperature. The absolute values of λ at 1.6 K show a clear trend that they decrease with the increase of the Al or Cu layer thickness.

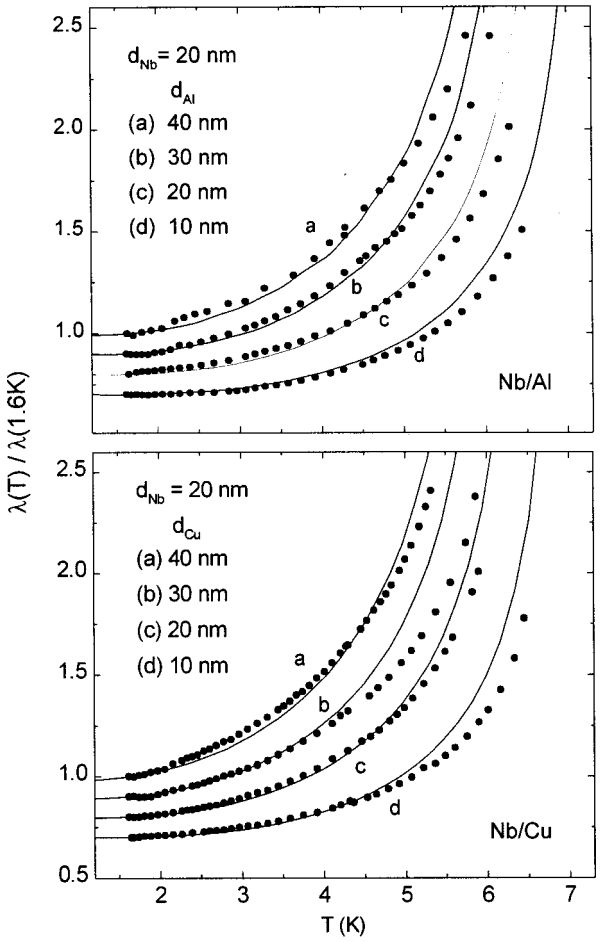

FIG. 4. Penetration depth $\lambda(T)$ for the Nb/Al (group A) and Nb/Cu (group B) bilayers. Dots and lines are the experimental and calculated results, respectively. Curves *b*, *c*, and *d* are successively shifted downwards by 0.1 on the vertical scale for clarity.

As a result of the proximity effect, the order parameters in both Nb and Al or Cu are expected to decrease with the increase of the Al- or Cu-layer thickness. The fact that λ in this situation also decreases arises from a decreasing resistivity ρ_{Al} or ρ_{Cu}, as can be seen from Eq. (13). In order to see this clearly, we use the expression $F_{S,S'}=\Delta_{S,S'}/(\omega_n+(T/T_c)\delta_{S,S'})$, which is suitable in the temperature region near T_c.[6] Inserting it into Eq. (13), one is led to the following expression:

$$\frac{1}{\lambda^2_{S,S'}}=\frac{\mu_0(\pi k_B T_c)^2}{\hbar(\pi k_B T)\rho_{S,S'}}\Delta^2_{S,S'}\psi'(1/2+\delta_{S,S'}), \qquad (15)$$

where $\psi'(x)=\Sigma_{n\geq 0}1/(n+x)^2$. Note that we have the order parameters normalized to $\pi k_B T_c$. Equation (15) shows the same result as first established by Deutscher *et al.*[24] in a different approach if we notice that $\delta_{S,S'}=\pm\hbar D_{S,S'}K^2_{S,S'}/(2\pi k_B T)$, where the upper and lower signs correspond to the S and S' layers, respectively.[6] Based upon this relation, Pambianchi *et al.*[2,7] have achieved a good agreement in fitting to the effective penetration depth change

$\Delta\lambda_{\rm eff}$ obtained from the microwave surface measurements. They found that the experimental $\Delta\lambda_{\rm eff}$ can be reproduced by assuming $\lambda^{-1}\sim\Delta$ or $\lambda^{-1}\sim\Delta/\sqrt{T}$, neglecting first the dependence on ψ'. From Eq. (15), we find that the film resistivities can influence λ in a direct way in addition to their influence on the order parameter itself. This can be seen clearly from our experimental results concerning the absolute values of λ.

The influence of film resistivity ρ (or the electronic mean free path l) on λ can be generally explained in the context of Pippard's nonlocal theory of superconductivity, in which a coherence length defined by $\xi_P^{-1}=\xi_0^{-1}+l^{-1}$ is introduced.[25,26] In a pure material where $l\to\infty$, ξ_P equals the BCS coherence length ξ_0. In this case, Pippard's equation reduces to the London equation in the local limit $\xi_P(=\xi_0)\ll\lambda$ with $\lambda^{-2}=\mu_0 e^2 n_S/m$, where n_S is the superconducting electron density. In a dirty material, on the other hand, Pippard's equation can reduce to a new London equation[26] if l is very small so that $\xi_P\sim l\ll\lambda$. In this case, we have $\lambda^{-2}=(\mu_0 e^2 n_S/m)(l/\xi_0)$. Thus λ will increase as l (or ρ) decreases (increases) even if n_S does not suffer a suppression. Considering the parameters discussed above, we can see that our experimental situation is close to this case.

Equation (15) shows the dependence of λ on the order parameter and film resistivity explicitly, but strictly speaking, it is applicable in the temperature range near T_c. In the whole temperature region below T_c, Eq. (13) should be used. In this case, the dependence of λ on the order parameters, given by Eqs. (11a) and (12a), is less direct. The solid lines in Fig. 4 are the results computed from the microscopic theory using the model I scheme (see Fig. 2), with the parameters listed in Table I. Comparing the experimental λ_e and theoretical λ_t at 1.6 K in Table I, we find that the deviations range from 9 to 20% and from 3 to 10% approximately for the samples of Group A and Group B, respectively. The agreement between theory and experiment for the absolute value as well as the temperature dependence of λ is reasonable considering that all the parameters used in our calculations are determined experimentally.

Figure 5 shows the temperature dependence of the order parameters of Group A samples. The dashed lines are the results in the Al layers that are spatially constant. The solid lines are the data in the Nb layers near the Nb/Al interface. The curve labels correspond to those of Nb/Al samples (Group A) in Fig. 4 and curves *e* are the data for the isolated Al and Nb films. From the figure, we see that by depositing an Al layer upon the Nb film, the order parameter in Nb is reduced while that in the Al layer is enhanced. With the increase of the Al-layer thickness, the order parameters in both layers decrease. Also in the temperature region where the λ data are shown in Fig. 4, the order parameters changes faster with temperature for thicker Al-layer samples, which is reflected in the $\lambda(T)$ characteristics in Fig. 4.

C. Penetration depths in the case of $R_B\neq 0$

The Nb/Al bilayers of Group A were sputtered in pure Ar so that the interface resistance R_B was approximately zero and $T_{c,\rm Al}$ was 1.2 K which was below the lowest temperature we could reach in our experiments. For the samples in Groups C to E, a small amount of O_2 gas was introduced into the sputter chamber right after the deposition of the Nb layers. In this way, we study the effect of a nonzero R_B on the experimental results and, with an elevated $T_{c,\rm Al}$ of 2 K, to see the $\lambda(T)$ behavior around $T_{c,\rm Al}$ of the Nb/Al bilayers.

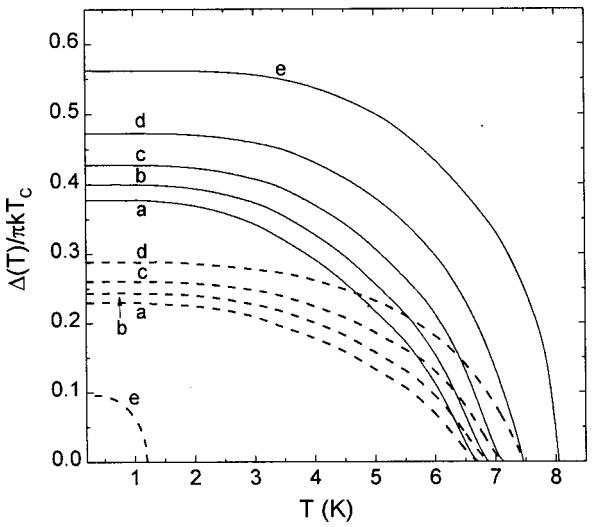

FIG. 5. Temperature dependence of the order parameters for the Nb/Al bilayers in Fig. 4 (group A). Dashed curves are the data for the Al layers and solid curves are data for the Nb layer near the Nb/Al interface. Curves from *a* to *d* correspond to those in Fig. 4. The bulk values are labeled as *e*.

Figure 6 shows the temperature dependence of λ, normalized to the values at 2.1 K, for the samples of Group C. For the sample with the interface oxidation time t_o of 5 sec, the $\lambda(T)$ curve is almost linear for the temperature range shown. With increasing t_o, a steplike, two-gap feature around $T_{c,\rm Al}=2$ K gradually develops. Such a feature becomes very clear for the sample with largest t_o of 300 sec.

These results might be anticipated from a simple physical consideration since for larger t_o and therefore larger R_B, the Nb/Al interface coupling is weaker. In this case, a smaller number of electrons in Al will condense into Cooper pairs

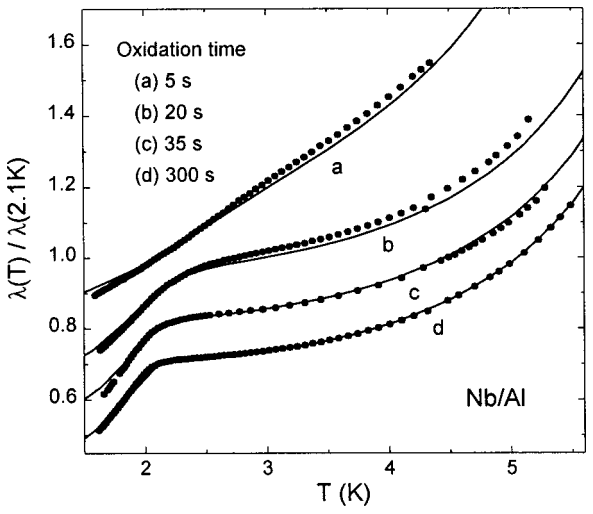

FIG. 6. Penetration depth $\lambda(T)$ for the samples of group C. Dots and lines are the experimental and calculated results, respectively. Curves *b*, *c*, and *d* are successively shifted downwards by 0.1 on the vertical scale for clarity.

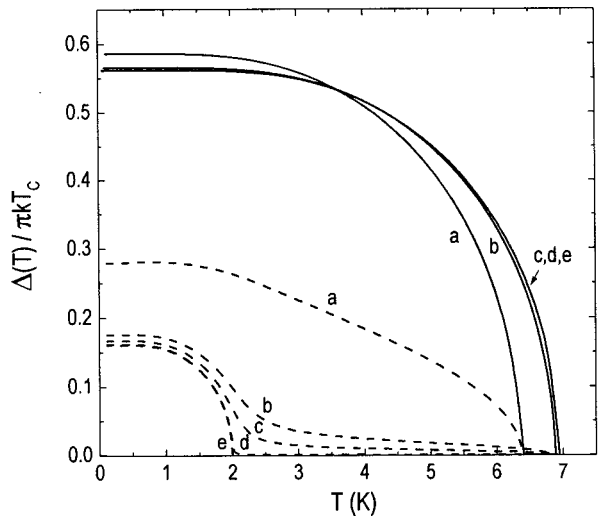

FIG. 7. Temperature dependence of the order parameters for the samples of group C in Fig. 6. Solid curves are the data for the Nb layers and dashed curves are the data for the Al layers near the Nb/Al interface. Curves from *a* to *d* correspond to those in Fig. 6. Curves labeled *e* are the bulk values.

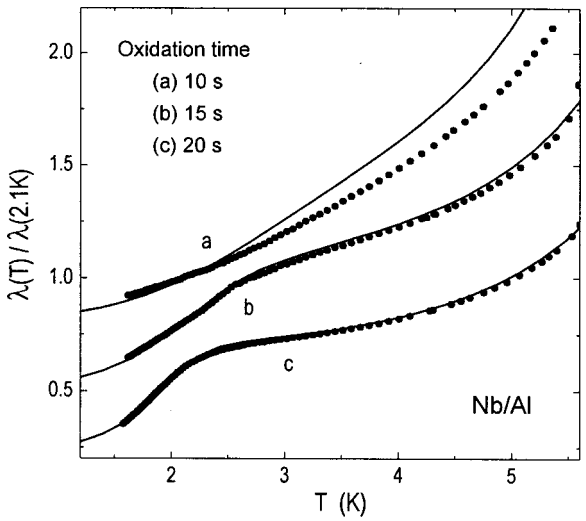

FIG. 8. Penetration depth $\lambda(T)$ for the samples of group D. Dots and lines are the experimental and calculated results, respectively. Curves *b* and *c* are successively shifted downwards by 0.2 on the vertical scale for clarity.

for $T>T_{c,\mathrm{Al}}$. When the temperature is lowered down through $T_{c,\mathrm{Al}}$, the change of Cooper pair densities in Al will be larger, which makes the penetration depth decrease faster. The solid lines in Fig. 6 are the theoretical $\lambda(T)$ calculated using the model II scheme. The parameters used for the calculations are listed in Table II. In Fig. 7, the temperature dependence of the order parameters in both Nb and Al layers of the samples in Group C are shown. The solid lines are the results in the Nb layers that are now spatially constant while the dashed lines are the results in the Al layers near the Nb/Al interface. As can be seen in the figure, for the sample with $t_o=5$ sec the variation of the order parameter with the temperature in the Al layer is slow near $T_{c,\mathrm{Al}}$. With increasing t_o, the order-parameter variation becomes faster around $T_{c,\mathrm{Al}}$ and gradually approaches curve e of the results of an isolated Al film.

From Table II, we can see that for the Group C samples, while increasing t_o up to 300 sec leads to a continuous increase of R_B, the bilayer properties including T_c and λ do not change much after t_o exceeds 35 sec (T_c even has a slight decrease in the case of $t_o=300$ sec due to the over-oxidation which results in a larger reduction of $T_{c,\mathrm{Nb}}$). The samples in Group D were prepared with a shorter range of t_o and also with a lower O_2 partial pressure which resulted in lower Al-layer resistivities. In Fig. 8, the experimental and theoretical results of $\lambda(T)$ for the samples of Group D are shown. Comparing the data of these two groups, we find that the λ_e values in Group C are very close to each other at 2.1 K, but those in Group D increase from 297 to 505 nm with t_o from 10 to 20 sec. The difference arises from the difference of the Al layer resistivities ρ_{Al}. ρ_{Al} in Group C is twice as large as ρ_{Al} in Group D. A larger ρ_{Al} means a shorter coherence length ξ_{Al}. A shorter ξ_{Al} in turn implies a smaller volume of the Al layer which is effective in screening the magnetic field. In addition, a large ρ_{Al} leads to a large λ in Al, as discussed above. Therefore for the samples of Group C, the Al layers have less effect on the values of λ and the Nb layers play a main role in determining the values at $T>T_{c,\mathrm{Al}}$. The values of λ are almost the same, since their Nb layer thicknesses are the same. But for the samples of Group D, with smaller ρ_{Al}, the roles of the Al layers on λ become important. In this case, λ increases with increasing t_o at $T>T_{c,\mathrm{Al}}$ because the screening becomes less effective in Al when the coupling between Nb and Al is weaker.

In Fig. 9, we show the interface resistance R_B versus the oxidation time t_o for the samples in Groups C and D. In logarithmic scales, they follow nicely a linear dependence. Such a dependence has been observed in the tunneling barrier formation through thermal oxidation on metal surfaces[27] and can be well-understood since the oxide thickness has a logarithmic dependence on t_o for a fixed O_2 pressure while the tunneling current has an exponential dependence on the oxide thickness.[28] The slopes of the lines, which can be affected by the oxidation pressure and temperature, are different. Technically, R_B has been used as an adjustable parameter in our theoretical fitting to the experimental T_c and λ with the above $R_B \sim t_o$ dependence as a constraint.

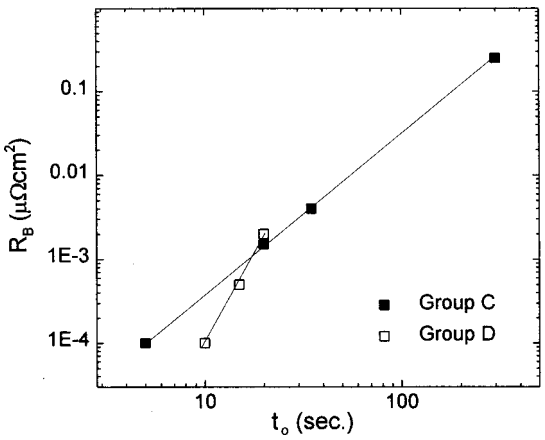

FIG. 9. Interface resistance vs oxidation time for the Nb/Al sandwiches in groups C and D. Solid lines are drawn as a guide to the eye.

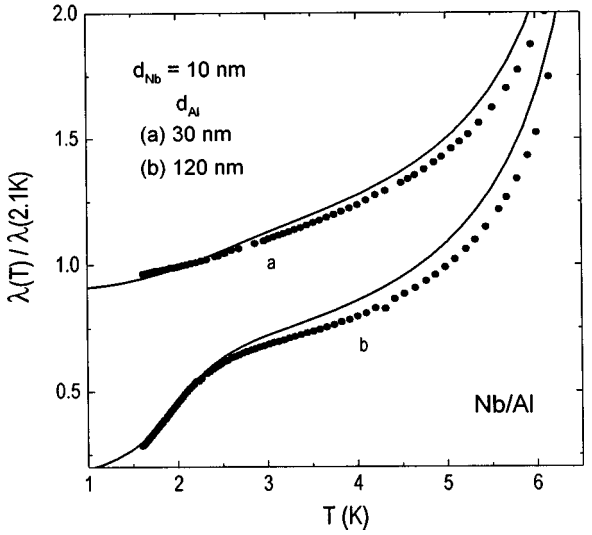

FIG. 10. Penetration depth $\lambda(T)$ for the samples of group E. Dots and lines are the experimental and calculated results, respectively. Curve *b* is shifted downwards by 0.5 on the vertical scale for clarity.

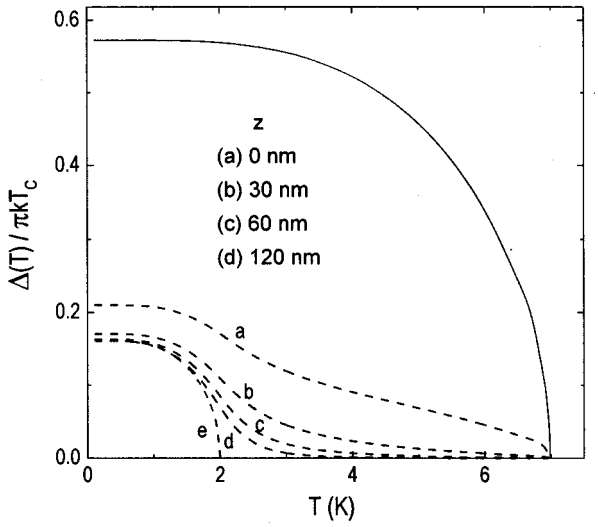

FIG. 11. Temperature dependence of the order parameter for the sample with $d_{\mathrm{Al}}=120$ nm in group E in Fig. 10. The dashed lines represent the results at four positions across the Al layer with z being measured from the interface into Al. The solid line indicates the order parameter in the Nb layer.

Besides the increase of oxidation time, the increase of the Al layer thickness can also result in the two-gap feature in the $\lambda(T)$ curve. The two samples in Group E have the same Nb-layer thickness and interface oxidation time, but their thicknesses of the Al layers are different. Figure 10 shows the temperature dependence of λ for these two samples. The solid lines in the figure are again the theoretical results. For curve a with the Al layer thickness of 30 nm, λ decreases with decreasing temperature but we do not see a clear change of the decreasing rate around $T_{c,\mathrm{Al}}$. The situation is different for curve b with the Al-layer thickness of 120 nm where we can see a clear two-gap structure near $T_{c,\mathrm{Al}}$. This result is expected because the volume in the Al layer that is affected by Nb layer through the proximity effect is in the order of several times of ξ_{Al}. As the Al-layer thickness becomes large, the volume of the Al layer that is less affected by Nb also becomes large. This volume of Al will have a faster increase of the superconducting electron densities (and therefore the screening effect) when the temperature is lowered down through $T_{c,\mathrm{Al}}$, and λ will decrease faster accordingly. The dashed lines in Fig. 11 show the temperature dependence of the order parameter at different positions in the Al layer in the case of curve b in Fig. 10. We can see that the results are very similar to those in Fig. 7 but from a to d the curves reflect the changes when the distance from the Nb/Al interface in Al increases while those in Fig. 7 reflect the changes when the coupling strength between the Nb and Al layers decreases. With the increase of the distance from the interface, the temperature dependence of order parameter in Al layer tends to the ''decoupled'' line *e* and can in principle reach it if the distance becomes infinite. Similarly, it is mainly the shape of $\Delta_{\mathrm{Al}}(T)$ which determines the shape of $\lambda(T)$ near $T_{c,\mathrm{Al}}$.

We note that the properties of the Nb/Al bilayers, for example, the order parameters, change in a continuous way as the temperature changes across $T_{c,\mathrm{Al}}$ in the microscopic theory. Our previous numerical results[6] indicate that $\Delta_{\mathrm{Al}}(z)$ decays exponentially with z near T_c. The decay length K^{-1} increases with decreasing T, but for the temperatures $T \ll T_c$, the decay is no longer exponential and becomes slower. The decay length K^{-1} does not have a divergent behavior near $T_{c,\mathrm{Al}}$. This continuous behavior can also be seen in Fig. 11 in which $\Delta_{\mathrm{Al}}(z)$ decreases always with increasing z around $T_{c,\mathrm{Al}}=2$ K. These results predicted by the microscopic theory are in contrast with those predicted by the phenomenological approach using $\Delta_{S'}(z,T) \propto \Delta_S(T)\exp(-K_{S'}z)$ and $\lambda^{-1}\sim\Delta$ or $\lambda^{-1}\sim\Delta/\sqrt{T}$ based upon Eq. (15). In the latter case, we have the decay length given by $K_{S'}^{-1}=\xi_{S'}/\sqrt{T/T_c}$ for $T_{c,S'}=0$, or $K_{S'}^{-1}=\xi_{S'}/\sqrt{\delta_{S'}(T/T_c)}$ for $T_{c,S'}>0$, which diverges as $T\to 0$ or $T\to T_{c,S'}$.

V. SUMMARY

In this work, we have systematically studied the magnetic penetration depth λ in superconducting Nb/Al and Nb/Cu bilayers. The absolute values of λ were measured by the two-coil mutual inductance technique. Results on the transition temperatures of the bilayers, their temperature dependencies of λ under the variations of the sample and material parameters were presented, and were compared with the model calculations from the microscopic theory. The agreement between theory and experiment is fair.

For a spatially homogeneous BCS superconductor, its $\lambda(T)$ behavior at low temperatures is known to have the form of $\sim 1+\sqrt{2\pi\Delta/k_BT}\exp(-\Delta/k_BT)$. This T dependence is essentially exponential and the $\lambda \sim T$ curve becomes very flat at low temperatures. For a superconducting SS' bilayer, the situation is quite different due to the spatially inhomogeneous properties along the direction perpendicular to the layer planes. Our results indicate that the presence of an Al or Cu layer on the Nb film can greatly affect the behavior of $\lambda(T)$ and lead to its rich characteristics. We have shown that the temperature dependence of λ usually follows a power

law, or sometimes a linear dependence, if the layer thicknesses are less than several times of $\xi_{S,S'}$ or when the interface resistance R_B is small (see Fig. 4 and curves a in Figs. 6, 8, and 10). A two-gap, steplike feature in the $\lambda(T)$ curve will develop around $T_{c,S'}$ $(T_{c,S}>T_{c,S'}\geqslant 0)$ with increasing R_B and with the S' layer thickness many times larger than $\xi_{S'}$ (Figs. 6, 8, 10). We found that the shape of $\lambda(T)$ is closely related to the shape of the order parameter $\Delta(T)$. This can be seen explicitly from Eq. (15) if the temperature is not too far away from T_c, and it remains basically true in the whole temperature range below T_c, as demonstrated from our numerical simulations based upon the microscopic theory.

In addition to the temperature dependence of λ, we also found a reasonable agreement between experiment and theory concerning the absolute values of λ (discrepancies arose primarily from the uncertainty of the transition temperatures of the Nb films, especially when an oxidation process was involved). The film resistivities in this respect were found to be important in determining the absolute values of λ.

ACKNOWLEDGMENTS

We thank Professor F. Z. Xu and Dr. H. Du for their kind help during sample preparations.

[1] M. S. Pambianchi, L. Chen, and S. M. Anlage, Phys. Rev. B **54**, 3508 (1996).
[2] M. S. Pambianchi, S. N. Mao, and S. M. Anlage, Phys. Rev. B **52**, 4477 (1995).
[3] L. V. Mercaldo, S. M. Anlage, and L. Maritato, Phys. Rev. B **59**, 4455 (1999).
[4] J. H. Claassen, J. E. Evetts, R. E. Somekh, and Z. H. Barber, Phys. Rev. B **44**, 9605 (1991).
[5] K. Kanoda, H. Mazaki, N. Hosoito, and T. Shinjo, Phys. Rev. B **35**, 8413 (1987).
[6] S. P. Zhao and Q. S. Yang, Phys. Rev. B **59**, 14 630 (1999).
[7] M. S. Pambianchi, J. Mao, and S. M. Anlage, Phys. Rev. B **50**, 13 659 (1994).
[8] $K_{S'}^{-1}$ can be independent of temperature if S' is a spin glass, as is found recently in Nb/CuMn bilayers in Ref. 3. In this work, we restrict ourselves to the cases where S' is a superconductor or a normal metal.
[9] G. Eilenberger, Z. Phys. B: Condens. Matter **214**, 195 (1968).
[10] K. Usadel, Phys. Rev. Lett. **25**, 507 (1970).
[11] A. T. Fiory, A. F. Hebard, P. M. Mankiewich, and R. E. Howard, Appl. Phys. Lett. **52**, 2165 (1988).
[12] R. F. Wang, S. P. Zhao, G. H. Chen, and Q. S. Yang, Appl. Phys. Lett. **75**, 3865 (1999).
[13] S. P. Zhao, H. Du, G. H. Chen, and Q. S. Yang, Appl. Phys. Lett. **72**, 3062 (1998).
[14] The samples in groups C and D were among the first in the resistivity measurements using photolithographic patterning and wet etching, which resulted in severe underetching. The resistivity data thus obtained were very much scattered. Here the exact data of ρ_{Al}, which lead to the reasonable fittings of both T_c and λ, are listed.
[15] M. Yu. Kuprianov and V. F. Lukichev, Zh. Éksp. Teor. Fiz. **94**, 139 (1988) [Sov. Phys. JETP **67**, 1163 (1988)].
[16] P. G. de Gennes and E. Guyon, Phys. Lett. **3**, 168 (1963).
[17] N. R. Werthamer, Phys. Rev. **132**, 2440 (1963).
[18] A. A. Golubov, E. P. Houwman, J. G. Gijsbertsen, V. M. Krasnov, J. Flokstra, H. Rogalla, and M. Yu. Kupriyanov, Phys. Rev. B **51**, 1073 (1995).
[19] A. A. Golubov, in *Superconducting Superlattices and Multilayers*, edited by Ivan Bozovic, Proc. SPIE Vol. 2157 (SPIE, Bellingham, WA, 1994), p. 353.
[20] There is a mistake in Eq. (21) of Ref. 6. On the right-hand side of that equation, 2π should be replaced by 4π, as it is now in Eq. (13) of this paper.
[21] The theoretical $T_{c,\mathrm{Cu}}$ is taken from R. Meservey and B. B. Schwartz, in *Superconductivity*, edited by R. D. Parks (Dekker, New York, 1969). This is for the convenience in the following λ calculation. Here the results will be only slightly different if the experimental $T_{c,\mathrm{Cu}}=0$ K is used instead.
[22] M. S. M. Minhaj, S. Meepagala, J. T. Chen, and L. E. Wenger, Phys. Rev. B **49**, 15 235 (1994).
[23] A. Sidorenko, C. Sürgers, T. Trappmann, and H. v. Löhneysen, Phys. Rev. B **53**, 11 751 (1996).
[24] G. Deutscher, J. P. Hurault, and P. A. van Dalen, J. Phys. Chem. Solids **30**, 509 (1969).
[25] M. Tinkham, *Introduction to Superconductivity* (McGraw-Hill, New York, 1996).
[26] P. G. de Gennes, *Superconductivity of Metals and Alloys* (Benjamin, New York, 1966).
[27] See, for example, J. P. Garno, J. Appl. Phys. **48**, 4627 (1977).
[28] E. L. Wolf, *Principles of Electron Tunneling Spectroscopy* (Oxford University Press, Oxford, 1985).